Pinch Oscillations in Electron-Hole Plasmas. II. Experiment

W. S. CHEN* AND B. ANCKER-JOHNSON
Boeing Scientific Research Laboratories, Seattle, Washington 98124 and
University of Washington,† Seattle, Washington 98124

(Received 2 June 1970)

Most of the measurements concern the spontaneous pinch oscillations that occur when the current exceeds a threshold value. Some properties of oscillations driven at subthreshold conditions are described also. The oscillations are characterized by several parameters: threshold current, amplitude, frequency, and wavelength. The dependency of the spontaneous oscillation properties on current, temperature, and time are reported. An applied longitudinal magnetic field has remarkable effects on the oscillations. In particular, the oscillations are stabilized at a critical magnetic field which depends on the current. The variations of the oscillation amplitude and the mode type with applied magnetic field are also shown. At subthreshold conditions, a driven pinch ($m=0$) oscillation can be readily launched in a pinched plasma; its spatial growth is reported. This type of oscillation is attenuated strongly by the application of a longitudinal magnetic field exceeding 50 G. In a prepinched plasma (low current levels), the driven helical mode ($m=1$) oscillation can be made to grow, if the appropriate magnetic field is applied. The results are divided into two groups for discussion, those results explained by the theory presented in the preceding paper and those not formally explained.

I. INTRODUCTION

Nonequilibrium electrons and holes capable of pinching can be produced by injection[1] from current-carrying contacts in p-type InSb and by high-field impact ionization[2] in p- or n-type InSb. Since these electron-hole plasmas are not required to neutralize fixed ionic charges they can readily engage in gross displacements such as occur during the onset of the pinch effect.[3]

Small-amplitude voltage oscillations accompanying pinching, with and without applied magnetic fields, have been reported by many authors.[1–8] Large and growing amplitude oscillations have also been observed in injected plasmas.[9] These scattered and incomplete experimental results do not give a complete picture of the pinch oscillations The purpose of this study is to investigate systematically the oscillations related to pinched electron-hole plasmas and so provide the basis for a more rigorous and satisfactory theory (see the preceding paper, hereafter referred to as I).

Oscillations in both injected and impact-ionized plasmas have been investigated in this study. The oscillations in pinched impact-ionized plasmas are characterized by relatively small amplitudes, high frequencies, and high threshold currents. Also, these oscillations usually are not reproducible from pulse to pulse. In contrast to the oscillations in n-type samples, those in p-type samples are reproducible, and hence results pertaining to injected plasmas only are included in this study.

The form of the pinch oscillations is assumed to be $\exp[i(\omega t+kz+m\theta)]$, where ω is the angular frequency, k is the wave vector along the z axis (current direction), m is the mode number in the azimuthal direction, and θ is the azimuthal angle. The oscillations which are independent of θ, $m=0$, are called the sausage mode.[10] In an electron-ion (gas) plasma, the $m=1$ mode is familiar as the kink instability during which the entire pinch column deforms into a single helix.[10] In electron-hole plasmas the $m=1$ mode has been extensively studied in the prepinched plasmas (that is, in plasmas conducting less than the critical current for pinching) which are subject to longitudinal magnetic fields.[3] These helical instability oscillations involve only a fraction of the solid-state plasma, in contrast to the self-destructive kink instability in gas plasmas. At higher values of m, the plasma in the pinch assumes the form of a multistranded cable. By using four probes which are located symmetrically around the sample, in a plane perpendicular to the current direction, the signals caused by each mode can be measured separately.

In Sec. II the sample preparation and the measurement procedures are described. Section III contains all the experimental results on the spontaneous oscillations and oscillations driven at subthreshold conditions. The amplitude, frequency, and wavelength of these oscillations are recorded for different conditions of current, temperature, and time. The effects of an applied longitudinal magnetic field are also reported.

In the discussion, Sec. IV, the experimental results are divided into two categories. In the first are the results which are explained by the theory presented in I. In the second are those results which are not predicted by the theory. At the end of this section, some possible applications of the oscillatory properties are mentioned.

II. EXPERIMENTAL PROCEDURE

A. Sample Preparation

Since not every sample produced the phenomena described in this paper, sample preparation is deemed very important. The following preparation procedure usually produced oscillations. Every sample that produced oscillations did so reproducibly, but why some did not has not been determined.

TABLE I. List of samples and their low-field properties.

Sample No.	Dimensions (mm³)	p_0 (10^{14} cm^{-3})	μ_0 (10^3 cm²/V sec)
W 377C-2W	1.16×1.16×10.1	3.97	8.25
W 377C-13W	1.0×1.0×9.86	4.5	8.0
W 377C-14W	1.0×1.0×9.86	4.2	8.5
W 377C-18W	1.0×1.0×9.25	4.16	8.25
W 478E-8J	0.9×0.9×9.9	8.1	8.1
W 486B-1W	1.0×1.0×9.7	7.6	7.6
W 354-H-2W	1.1×1.1×10	1.33	8.56

Samples are cut in a parallelepiped shape from unoriented single crystals with a wire saw. To ensure that all surface damage introduced by the cutting is removed, the samples are polished down at least 0.2 mm on each side in a 0.3-μm alumina slurry and then etched in a solution of 2.1 ml distilled water, 42.9 ml 88.4% lactic acid, and 4.5 ml 70% nitric acid for 5–10 min at ~40°C. Contacts are alloyed in an atmospheric environment onto surfaces so prepared with the aid of a small amount of Divco 335 acid flux. To achieve high injection in p-type samples, the current contacts are alloyed onto the ends with 80% In+20% Cd and 99% In+1% Te, respectively, to form a p^+pn structure. Pure In is used on all the side voltage-probe contacts. Sandblasting the surfaces after the contacts are made does not influence the pinch oscillation characteristics.

Table I lists all the samples and their low-field properties as measured at 77 K.

B. Measurements

Since the general perturbations which are propagated by the pinch may be characterized by $\exp[i(\omega t+kz+m\theta)]$, the oscillations caused by each mode can be measured separately by using a four-probe system. If four probes are attached to a sample in a plane $z=z_0$ as shown in Fig. 1 and if the azimuthal angle θ is chosen to be zero at probe No. 1, the voltage measured by each probe is

$$V_n=V_{0m}\exp\{i[\omega t+k_mz_0+\tfrac{1}{2}(n-1)m\pi]\}. \quad (1)$$

Table II shows the signals associated with the $m=0$, 1, and 2 modes which can be measured by different combinations of probes. From the table, it can be seen that the $m=0$ mode oscillation can be measured separately from the other modes by connecting the four probes together $(V_1+V_2+V_3+V_4)$; the $m=1$ mode by subtracting signals from opposite probes $(V_1-V_3$ and $V_2-V_4)$; and the $m=2$ mode by the combination $(V_1+V_3)-(V_2+V_4)$.

If an oscillation is caused by a running wave, signals caused by each mode have the same amplitude independent of z, whereas the time phase shift is dependent on z. According to Table II, the measured V_1-V_3 and V_2-V_4 associated with the $m=1$ mode at a given position have $\frac{1}{2}\pi$ time phase difference between them. This is the case for the $m=1$ oscillation measured in high magnetic fields as discussed in Sec. III A 5.

If an oscillation is a standing wave, the signal associated with the $m=0$ mode, measured by $V_1+V_2+V_3+V_4$, has the form $4V_{00}\exp(i\omega t)\sin k_0z_0$. Therefore, the amplitude, not the time phase, of this signal changes with probe position, as described in the wavelength measurements, Sec. III A 4. Similarly, the signals of V_1-V_3 and V_2-V_4 which are used to study the $m=1$ mode oscillation assume the form $2V_{01}\exp(i\omega t)\sin(k_1z_1)$ and $2V_{01}\exp(i\omega t)\cos(k_1z_0)$, respectively. For determining the wavelength of the $m=1$ mode, Sec. III A 4, instead of measuring either V_1-V_3 or V_2-V_4 alone, the signal $(V_1-V_3)/(V_2-V_4)$ is measured as a function of probe position along the sample, because this signal shows a distinctive peak as $V_2-V_4=0$.

Since the amplitude of the $m=2$ mode is found to be very small compared with the $m=0$ or $m=1$ modes, any slight irregularities in the probes, such as an asymmetry in their position, makes detection of the signal, $(V_1+V_3)-(V_2+V_4)$, to separate the $m=2$ modes from the other modes, extremely difficult.

The experimental arrangement is shown in Fig. 2. Power is applied for 1.5 to 4.5 μsec by a transmission-line pulse generator whose repetition rate is set between 15 and 30 Hz. The sample is either immersed in a liquid-nitrogen bath or located in a variable-temperature Dewar whose ambient can be changed from 4.2 K to room temperature.

The spontaneous oscillations are studied while the rf generator (Fig. 2) is disconnected from the sample. Each of the potential probes along the sample sides has a 5-kΩ (at 77 K) isolation resistor located very close to the sample and a 50-Ω termination at the opposite end of the probe line. Voltages and currents

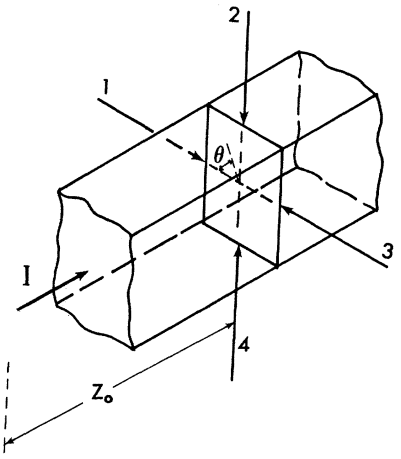

FIG. 1. Schematic of the voltage probe locations.

TABLE II. Signals obtained from various probe combinations as caused by the $m=0$, 1, and 2 modes.

Probe combination	$m=0$	$m=1$	$m=2$
$V_1+V_2+V_3+V_4$	$4V_{00}\exp[i(\omega t+k_0z_0)]$	0	0
V_1-V_3	0	$2V_{01}\exp[i(\omega t+k_1z_0)]$	0
V_2-V_4	0	$2V_{01}\exp[i(\omega t+k_1z_0+\pi/2)]$	0
V_1-V_2	0	$\sqrt{2}V_{01}\exp[i(\omega t+k_1z_0-\pi/4)]$	$2V_{02}\exp[i(\omega t+k_2z_0)]$
V_2-V_3	0	$\sqrt{2}V_{01}\exp[i(\omega t+k_1z_0-\pi/4)]$	$-2V_{02}\exp[i(\omega t+k_2z_0)]$
$(V_1+V_3)-(V_2+V_4)$	0	0	$4V_{02}\exp[i(\omega t+k_2z_0)]$

are monitored by broad-band oscilloscopes. The wavelengths of the various spontaneous oscillation modes are determined by measuring the potential along the sample length with a set of four movable probes which have a spatial resolution of ≤ 15 μm.

The arrangement for the excitation and detection of waves when the current level is below the threshold of the spontaneous oscillations is shown in Fig. 2. The rf signal generator provides signals either in phase or 90° out of phase (latter case shown in Fig. 2) so that the $m=0$ or $m=1$ waves may be launched. Launched waves are detected in the same manner as spontaneous oscillations.

III. EXPERIMENTAL RESULTS

A. Spontaneous Oscillations

When the current through the samples reaches a threshold level well above the threshold for pinching of the injected plasma, spontaneous oscillations are observed on the voltage and current. Measurements of these oscillations under various conditions are presented in the following sections.

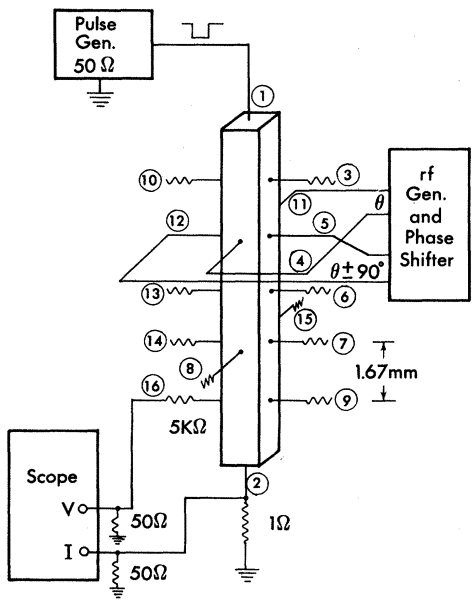

FIG. 2. Schematic arrangement of the experimental setup. The rf generator and phase shifter are used only in driven oscillation measurements.

1. Conduction Characteristics

The conduction characteristics measured at four different temperatures, 4.2, 20, 60, and 84 K, are shown in Fig. 3. The *I-E* curves exhibit the typical form: Ohmic conduction at low fields, strongly superOhmic conduction during injection, and then a reduction in conduction attributed to pinching. At a definite current threshold, well above the threshold for pinching, oscillations occur. The *I-E* curve envelopes in the high-field regions of Fig. 3 result from the variation in the phase of the voltage and current oscillations at the sampling time as the applied voltage is raised. The oscillograms in Fig. 3 show the oscillation of voltage and current at the levels marked on the *I-E* curves. It can be seen that both the amplitude and frequency of the oscillations are strong functions of current. Details are discussed in the following sections.

At temperatures ≤ 77 K, a low-frequency ($\sim$2 MHz) oscillation is superimposed on the usual oscillations in some samples [note oscillogram I in Fig. 3(b)]. The amplitude of such low-frequency oscillations increases as the temperature decreases.

The measured threshold current I_{th} of the spontaneous oscillations varies with temperature as shown in Fig. 4. The threshold current shows a minimum value at $\sim$50 K. This curve is similar to the temperature dependence of the reciprocal of the hole mobility (or ambipolar mobility) which has a maximum value at $\sim$50 K.[11] The so-called critical pinch current I_c (the current at which the differential resistance decreases after injection) has approximately the same temperature dependence as I_{th}, Fig. 4.

2. Amplitude of Oscillations

The peak-to-peak amplitude of the pinch oscillations relative to the electric field strength (percentage of modulation) is a function of current and electron-drift distance. Typical modulations observed at 77 K are shown in Fig. 5. The electric field strength at a given plane, e.g., that defined by probes 7, 8, 14, and 15, is modulated by the $m=0$ sausage mode up to 38%, but only $\sim$2% by the helical modes, for which $m>0$. These curves also show that a considerable growth in the

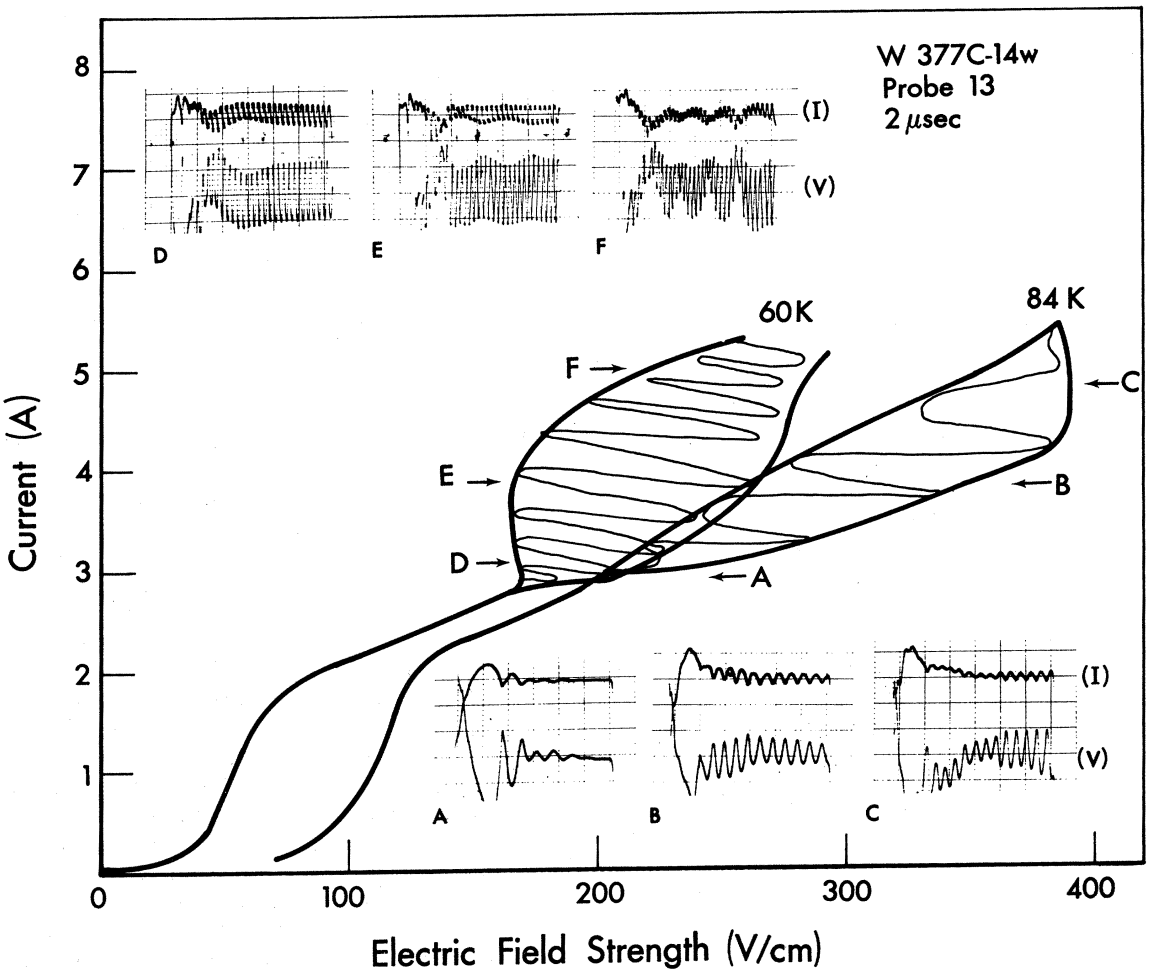

(a)

FIG. 3. (a) Conduction characteristic at four different temperatures. Measurements are made by sampling the current and voltage at 2 μsec after the beginning of the pulse. The oscillograms show the oscillations on the top of the current and voltage pulses at the levels marked on the *I-E* curves. Horizontal scale=0.5 μsec/div. Current scale=0.38 A/div; voltage scale=9 V/div for *A* and *C*, 18 V/div for *B*, and 10 V/div for *D*, *E*, *F*. (b) Conduction characteristic at four different temperatures. Measurements are made by sampling the current and voltage at 2 μsec after the beginning of the pulse. The oscillograms show the oscillations on the top of the current and voltage pulses at the levels marked on the *I-E* curves. Horizontal scale=0.5 μsec/div. Current scale=0.32 A/div for *G*, *H*, *I* and 0.93 A/div for *J*, *K*, *L*; voltage scale=13 V/div for *G* and *H*, 25 V/div for *I*, and 43 V/div for *J* and *K*, 108 V/div for *L*.

amplitude of the oscillations relative to the electric field strength occurs in the direction of electron drift.

The percentage of modulation caused by the $m=0$ mode oscillation is not always as smooth a function of current as illustrated in Fig. 5. Some examples exhibit modulation with distinctive peaks as a function of current (as will be discussed in connection with Fig. 9 below); however, all the measurements at 77 K have these features in common: (1) The onset of the oscillations occurs at a well-defined threshold I_{th}; (2) the cutoff of the oscillation, however, does not occur at a sharply defined current. Indeed, in some samples, the oscillations persist as current is increased until the oscillations become irregular.

The ambient temperature not only affects the threshold current of the oscillations but also influences their amplitude and its dependence on current. The maximum percentage of modulation caused by the $m=0$ mode oscillation has its highest value ($\sim$50%) at 4.2 K, as shown in Fig. 6 for the particular sample measured in such detail. The percentage drops to $\sim$23% at 20 K and then has a plateau in the temperature range 20–65 K. At higher temperatures the percentage of modulation decreases monotonically. The current levels at which the modulations are maximized are marked on the modulation curve in Fig. 6. The temperature dependence of the current levels at which maximum modulation occurs is very similar to the $I_{th}(T)$ characteristics shown in Fig. 4.

The percentage of modulation at elevated tempera-

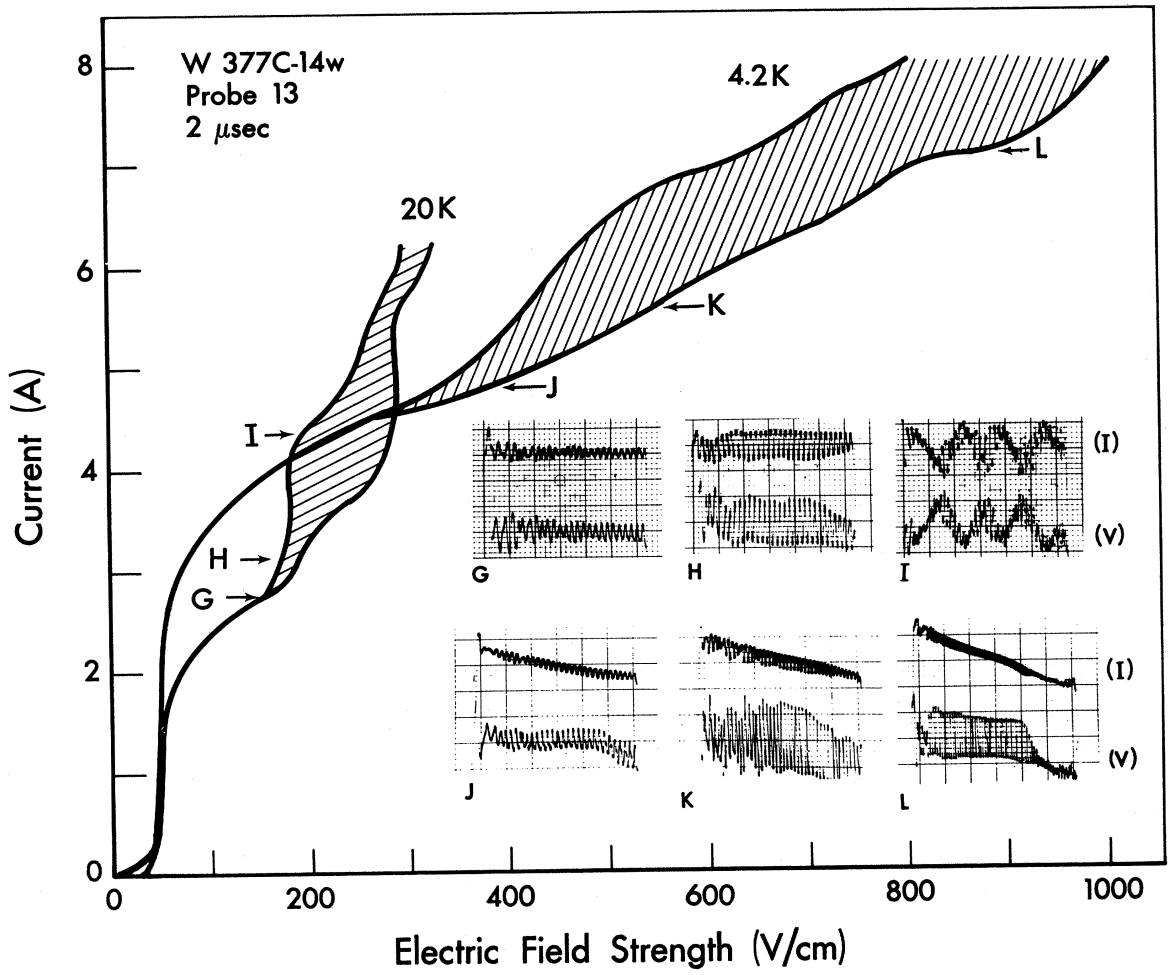

(b)

FIG. 3.—Continued

tures (>77 K) for this sample (*W* 377*C*-14*W*) is a smooth function of current with only one maximum similar to the curves in Fig. 5. However, at lower temperatures (4.2–77 K) the single maximum splits into multiple peaks with shallow valleys between them. The dependence of the half-amplitude width of the full curve (percentage of modulation as a function of current) on temperature is shown in Fig. 6. This dependence is generally similar to the dependence of the change in percentage of modulation with temperature.

The inset of Fig. 7 shows the percentage of modulation at 77 K as measured along the sample length from cathode to anode. The straight lines in this semilog plot show how the percentage of modulation, α, varies with distance x, namely, $\alpha(x)=\alpha_0 \exp(\gamma x)$, where γ is defined as a spatial growth rate of the percentage of modulation caused by the $m=0$ mode oscillations. The variations of γ with current and time after the onset of power are shown in Fig. 7. Near the cathode (upper curves) the growth rate is constant, ~ 2 cm^{-1} (19 dB/cm), over the entire current range as observed soon after the application of a voltage step, but γ decreases with current at later times. The growth rates near the anode are considerably less and change with current in a complex way, as shown by the lower curves in Fig. 7. This small magnitude of γ in the anode region does not occur in all samples; in *W* 354-*H*-2*W*, which has a lower threshold (2.95 A) for spontaneous oscillations, γ is as large in the anode as cathode regions, 1.96 cm^{-1} (17 dB/cm) at 2.97 A and 1.2 μsec.

3. *Frequency*

Measurements show that the frequency of the spontaneous pinch oscillation varies with ambient temperature, current, and the time measured after the application of a voltage step. A remarkable feature is that the $m=0$ and $m>0$ modes always oscillate with identical frequencies.

The frequency at 77 K is a linear function of current at constant time and an exponentially decreasing

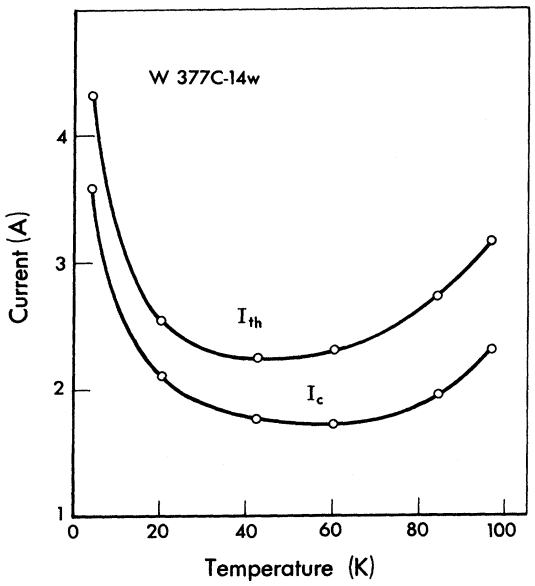

FIG. 4. Threshold current for the spontaneous oscillation and the critical current for pinching as a function of temperature.

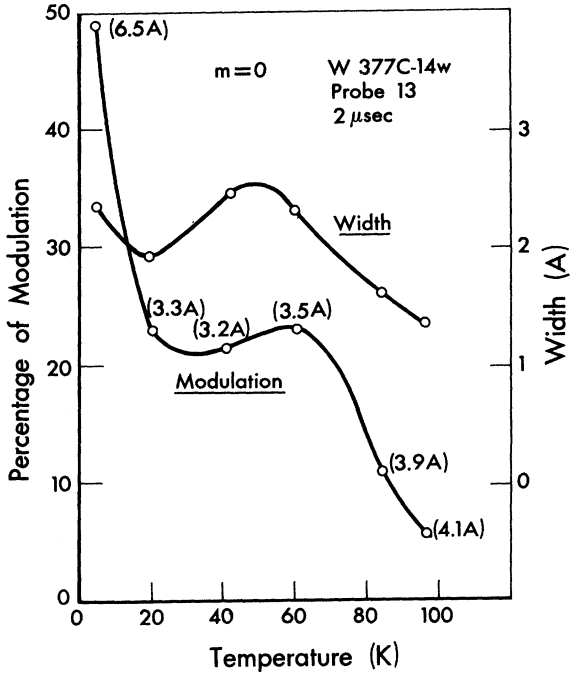

FIG. 6. Maximum percentage of modulation, and the half-amplitude full-width of the modulation versus current curve for the $m=0$ mode, as a function of ambient temperature. The maximum modulation occurs at the current levels marked in the parentheses.

function of time measured from the beginning of the pulse, as shown in Figs. 2 and 6 of I. This behavior is well explained by the model introduced in I. The linear relationship is observed throughout the temperature range 4.2–100 K.

In Fig. 8 the slope of the frequency-current relationship df/dI, and the threshold frequency are presented

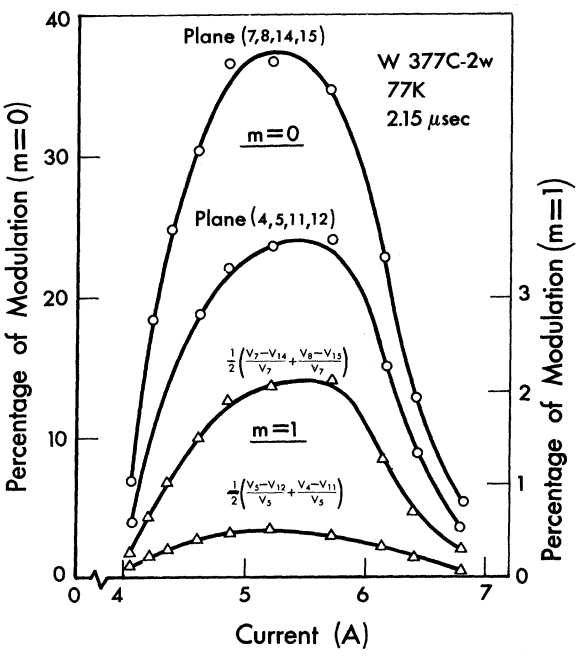

FIG. 5. Percentage of modulation for the $m=0$ and $m=1$ oscillations as a function of current.

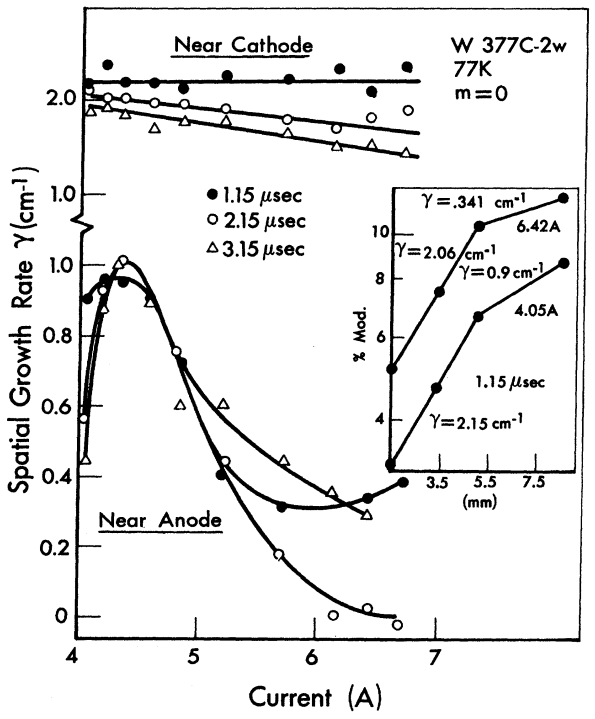

FIG. 7. Spatial growth rate near the cathode and near the anode as a function of total current. The inset shows the measured percentage of modulation as a function of distance from the cathode on a semilogarithmic scale.

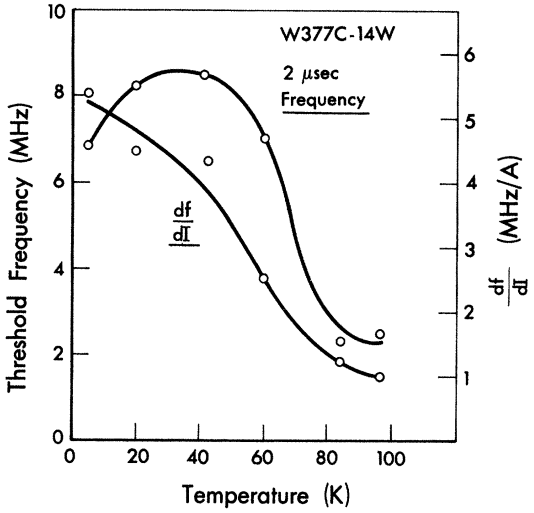

FIG. 8. Threshold frequency, and the rate of change of frequency with respect to current, df/dI, as a function of the ambient temperature.

as functions of the ambient temperature. The df/dI curve has its highest value, 5.3 MHz/A, at 4.2 K and decreases with temperature monotonically. The threshold frequency has a peak value of 8.6 MHz at 33 K. At elevated temperatures (>80 K) the threshold frequency becomes constant at 2.3 MHz.

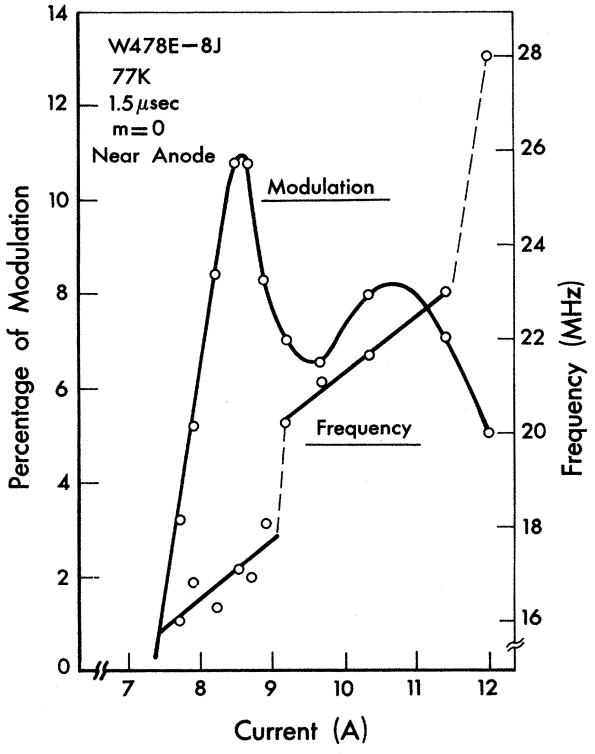

FIG. 9. Frequency as a function of current showing a discontinuous jump in between peaks in the modulation curve.

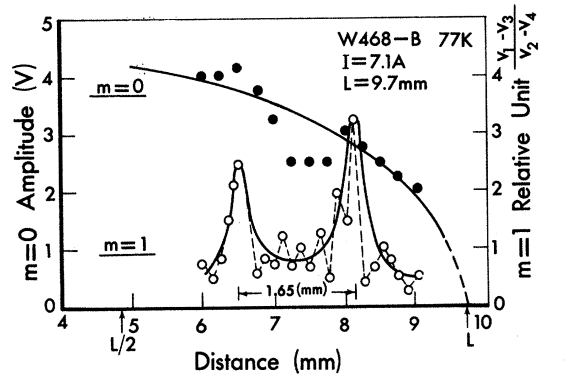

FIG. 10. Measurements of the $m=0$ mode wavelength, as made by connecting all four probes together, and the $m=1$ mode wavelength as detected by subtracting the signals between opposite probes.

As mentioned in Sec. III A 2, the percentage of modulation caused by the $m=0$ mode oscillation may show several peaks as a function of current. In Fig. 9, the percentage of modulation as a function of current shows two distinct peaks. Associated with each peak is a linear dependence of frequency on current; the frequency shows a discontinuous jump at the current levels which separate the modulation peaks. There is probably another peak in the percentage of modulation at higher current levels than measured (in order not to get into the destructive thermal pinch range), since the frequency abruptly increases again at 12 A, as shown in Fig. 9. Even though the peaks in the modulation-current curves are only barely distinguishable in

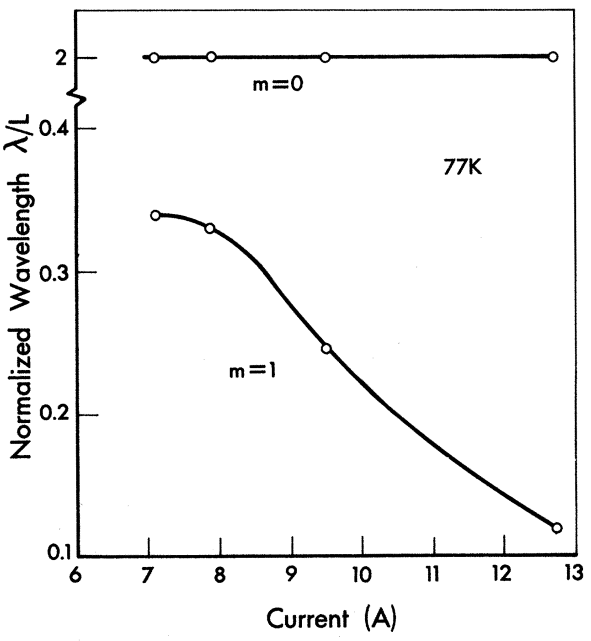

FIG. 11. Wavelength normalized to the sample length as a function of total current for both the $m=0$ and $m=1$ modes.

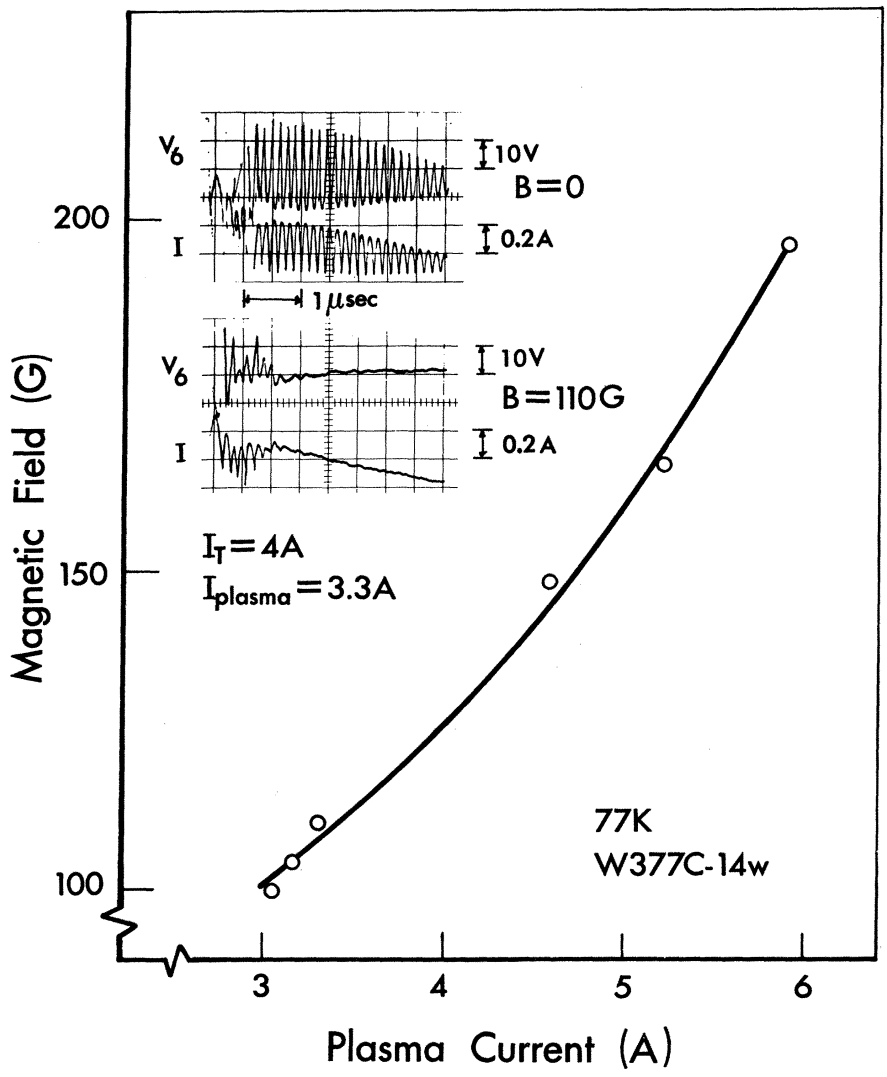

FIG. 12. Critical longitudinal magnetic field at which the oscillation is stabilized as a function of plasma current = I(total) − I(Ohmic). The oscillograms show the oscillatory behavior of the voltage and current with and without an applied magnetic field.

some samples, the frequency between peaks always discontinuously increases. These results are in agreement with previous work[9] which, however, reported a feature not observed in the present work, namely, the occurrence of essentially zero amplitude between maxima and under some circumstances a discontinuous *decrease* in frequency with increasing current.

4. *Wavelength*

A continuously translatable probe device makes possible wavelength measurements of the pinch oscillations. If an oscillation is characterized by $\exp[i(\omega t+kz+m\theta)]$, probing along the sample length should produce a continuously phase-shifted voltage. Measurements detect no phase shift; instead, the amplitude of the oscillations varies along the sample length. Thus the oscillation is caused by a standing wave. Care must be exercised in using the translatable probes to determine the wavelength, because both the amplitude and frequency of the oscillations are very sensitive to probe position. Since the probes unavoidably load the sample, they disturb the electric field. Consequently, the oscillations change frequency and amplitude as the probes are moved along the sample. Fortunately the loading effect proves to be negligible when the probes are used sufficiently far away from the cathode. Therefore, all measurements are made in the anode half of the samples.

In Fig. 10 the oscillation amplitude, as detected with the four probes shorted together (top curve), is shown as a function of distance from the cathode at 77 K. Clearly the $m=0$ mode, sausage-type oscillation, is a standing wave with its half-wavelength equal to the sample length, labeled L on the abscissa. In the same

figure (lower curve), the amplitude of V_1-V_3, the difference in voltage detected on probes 1 and 3, as normalized to the voltage difference measured at probes 2 and 4 is also plotted as a function of distance. These results yield the wavelength of the $m=1$ helical mode.

The measured wavelengths, normalized to the sample length, for both $m=0$ and $m=1$ modes are reproduced in Fig. 11 as functions of current. The wavelength of the $m=0$ mode is equal to twice the sample length independent of current. The wavelength of the $m=1$ mode is much smaller than the wavelength of the dominant $m=0$ mode. Furthermore, the normalized wavelength of the $m=1$ helical mode decreases with current and tends to saturate to a value of ~ 0.35 at lower current levels. Higher-mode ($m>1$) oscillations are also present in very small amplitude, but their wavelengths have not been measured because the separation of the higher modes from the $m=0$ and $m=1$ modes is very difficult to accomplish.

It is interesting to compare these results with those of Dubovoi and Shanskii,[12] who measured the wavelength of the helical instability ($m=1$) mode in Ge as a function of the magnetic field. They found the wavelength is equal to one-half the sample length in low magnetic fields and decreases with increasing magnetic field.

5. *Response to Longitudinal Magnetic Fields*

The amplitude of the spontaneous pinch oscillations varies with applied longitudinal magnetic field. The oscillations are stabilized when a magnetic field of the proper magnitude is applied. The oscillograms reproduced in Fig. 12 illustrate the stabilizing effect. The upper picture shows the voltage and current oscillations in the absence of an applied magnetic field. In the lower picture the effect of a critical magnetic field, 110 G in this case, is seen: The oscillations virtually disappear.

In the course of determining the critical magnetic field, it was observed that the stabilizing effect starts at the end of the pulse and appears toward the beginning as the applied magnetic field is increased.

The critical field as a function of current is also shown in Fig. 12. Its magnitude, 100–200 G, spans the calculated self-magnetic field, $B_\theta=\mu^0 I/2a$, as estimated by assuming the radius of the pinch column, a, to be $\sim 5\times 10^{-3}$ cm.[13]

The amplitudes of the spontaneous pinch oscillation for the $m=0$ and $m>0$ modes are functions of the applied magnetic field. This is demonstrated by Fig. 13. At a current level, ~ 4 A, just exceeding the threshold for oscillation, the amplitudes of both the $m=0$ and $m>0$ modes decrease monotonically with the longitudinal magnetic field. When the critical magnetic field is reached, the oscillations are completely stabilized. At current levels appreciably higher than the threshold (two are shown in Fig. 13), the amplitude of the oscillations changes with applied magnetic field in a

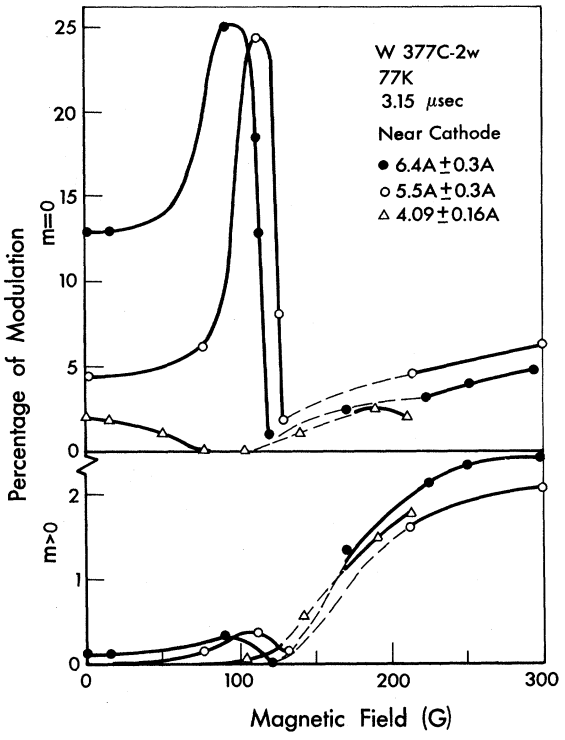

FIG. 13. Percentage of modulation caused by the $m=0$ mode (upper) and $m>0$ mode (lower) oscillations, as a function of applied longitudinal magnetic field at three different current levels.

quite different way compared to the dependence at low-current levels. The percentage of modulation caused by the oscillations is greatly enhanced as the magnitude of the applied magnetic field is increased, and a sharp decrease in the modulation is observed as the magnetic field approaches the critical value. Thereafter, the stabilization of the oscillations persists for a range of only a few tens of gauss. Further increase in the longitudinal magnetic field causes the plasma to become turbulent at all current levels. The oscillations are then noisy and unstable. This turbulent region is indicated in Fig. 13 by broken lines. At still higher magnetic fields, stable oscillations are again observed in both $m=0$ and $m>0$ modes as the solid curves show in Fig. 13. The amplitudes of the stable $m>0$ oscillations in the high magnetic fields are comparable to the $m=0$ mode oscillation in the same magnetic field range and are much greater than the amplitudes of $m>0$ modes in the low magnetic field range ($B<B_c$).

Detailed results show that at high magnetic fields the voltage observed by subtracting the signals from opposite probes in a plane have approximately equal amplitudes and 90° phase shift relative to each other. This proves that the helical waves excited in a magnetic field greater than B_c are traveling waves, which may be

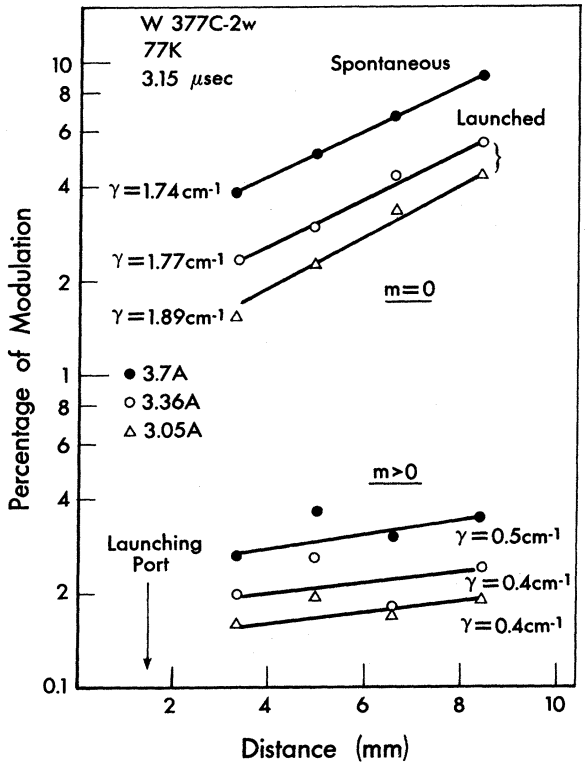

FIG. 14. Percentage of modulation caused by a driven $m=0$ mode oscillation, plotted as a function of distance from the cathode on a semilog scale at two current levels. The spontaneous oscillation at a current level of 3.7 A is also plotted here for comparison. Oscillations with $m>0$, though not launched, are also excited as shown by the lower curves. The growth rate γ associated with each curve is calculated from the slope.

characterized by $\exp[i(\omega t+\theta+kz)]$, in agreement with previous results,[14] and that they are not standing waves as are the small amplitude $m>0$ pinch oscillations in the absence of an applied magnetic field.

B. Driven Oscillations

At current levels below the threshold for spontaneous oscillations, waves driven by an rf source can be launched in the sample. Results of the measurements will be shown both with and without applied longitudinal magnetic fields. Two current regions corresponding to pinched and prepinched plasmas are discussed separately in the following sections.

1. Pinched Plasma

In the absence of a longitudinal magnetic field, an $m=0$ mode oscillation can be readily stimulated in a pinched plasma carrying a current just below the threshold for spontaneous pinch oscillations. The launching port is made by shorting two opposite probes (e.g., No. 3 and No. 10, Fig. 2) in a plane near the cathode. An rf signal generator, connected to the launching port, is frequency tuned to produce maximum oscillation amplitude at probes nearer the anode. Shown in Fig. 14 are the amplitudes of the launched oscillations relative to the electric field strength, as a function of distance from the cathode at two current levels, 3.05 and 3.36 A. The percentage of modulation caused by the launched $m=0$ oscillation grows exponentially along the sample length with growth rates as high as 1.89 cm^{-1} (16 dB/cm). The driven frequencies which produce the maximum growth at all current levels are very close to 5.9 MHz, which is slightly less than the frequency at the beginnlng of spontaneous oscillation. Spontaneous oscillation growth at a current level of 3.7 A, which is just above the threshold value, is also shown in the figure for comparison. The growth rate, 1.74 cm^{-1}, in the case of the spontaneous oscillation is about the same as the growth rate of launched oscillations. Although only the $m=0$ mode is launched, a small percentage of $m>0$ modes is also excited with much lower growth rates as the lower curves in Fig. 14 show.

In I the time dependence of the frequencies of the spontaneous oscillations is shown. In contrast, the driven oscillations are constant in time. Two oscillograms showing the driven and spontaneous oscillations are reproduced in Fig. 15 for comparison. In the case of the driven oscillation, the frequency is constant at 5.9 MHz throughout the pulse and the amplitude grows slowly with time. However, in the spontaneous case, the frequency changes from 6.25 MHz to 5.9 MHz and the amplitude varies with time in quite a different manner. For a given current below the spontaneous threshold, the amplitude of driven oscillations is a function of frequency with a resonance characteristic which has a broad bandwidth of $\sim$2 MHz for a 2-μsec pulse duration.

In the presence of longitudinal magnetic fields, previously reported experimental results[14] show that the $m=0$ mode oscillations can be launched in the pinched

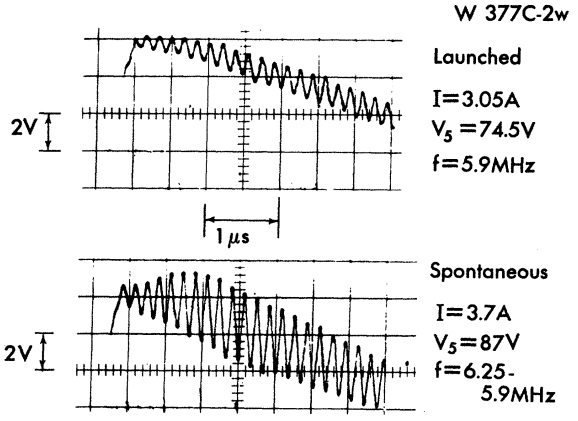

FIG. 15. Oscillograms showing launched and spontaneous oscillations as functions of time.

plasma only in a limited range of magnetic field, <35 G. This is due to the stabilization effect of the magnetic field as described in Sec. III A 5.

Attempts to launch the $m=1$ helical mode in a pinched plasma both in the presence and absence of an applied magnetic field were unsuccessful. In both cases, the launched oscillations are strongly attenuated along the sample length. In principle, the driven $m=1$ helical mode can be made to grow when a sufficiently high longitudinal magnetic field is applied. However, as shown in Fig. 13, the pinched plasma goes through a turbulent region to a spontaneous excited helical instability region as the magnetic field is increased. Therefore, in the pinched plasma the launched $m=1$ oscillations cannot grow in low magnetic fields and the launched oscillations are masked by the turbulence or spontaneous oscillations in the high-magnetic-field region.

2. *Prepinched Plasma*

When the current level is below the pinch threshold, the $m=0$ sausage-mode oscillations are strongly attenuated both in the presence and absence of longitudinal magnetic fields. Single helix waves can be launched and made to grow when sufficiently large magnetic fields are applied. The measured growth rates of these launched $m=1$ waves as a function of current, frequency, and magnetic field have been reported previously.[14] Growth rates as high as 80 dB/cm have been attained with $B<400$ G for frequencies in the tens of MHz range.

IV. DISCUSSION

In the course of this study a great deal of data have been collected. The results are grouped into two categories for discussion. In the first, those results which can be explained by the theory presented in I are discussed. In the second, those results which are not predicted by the theory of I are discussed. Finally, some possible applications of the oscillatory phenomena are mentioned.

A. Results in Agreement with Theory

The theory predicts growing $m=0$ mode oscillations in the long-wavelength limit in agreement with the measurements, Figs. 5 ($m=0$ is dominant), 7 (it grows), and 11 (the wavelength has the maximum possible magnitudes).

In the theory the temperature dependence of mobility is assumed to be $T^{-3/2}$, which is only valid at temperatures $\gtrsim 100$ K.[11] Hence, the low-temperature data cannot be compared with theory quantitatively. However, some qualitative comparisons can be made. The variation of the threshold frequency with temperature, Fig. 8, has a maximum at ~ 40 K, and so resembles the variation of electron mobility with temperature. This is in qualitative agreement with theory: Since the threshold current I_{th} of the spontaneous oscillations varies only weakly with the ambient temperature, namely for $4 \leq T \leq 100$ K, $I_{th}=2.3$–4.3 A (Fig. 4), it can be considered constant throughout the temperature range. The electric field strength at the threshold also varies only by a factor of ~ 2 throughout the temperature range. The only variables remaining at threshold in the expression for frequency, Eq. (28) of I, are then time and electron mobility. Hence, at a given time, the frequency is proportional to the mobility $\mu(T_0)$, if the mobility $\mu_0 T_0^{-3/2}$ in Eq. (25), is changed to an implicit function of temperature $\mu(T_0)$. Thus, the similarity in the temperature dependence of frequency and mobility is a consequence of the magnetothermal pinch theory.

As discussed in I, the value of the growth rate Γ must be very close to zero if the growth is not to be unreasonably large. Hence, according to Eq. (26) in I, $\Gamma \sim \mu(T_0) \times$ (a small quantity). Since the amplitude of oscillation is proportional to Γ, the amplitude variation with temperature should have the same general form as the mobility dependence on temperature. As shown in Fig. 6, the temperature variation of the modulation in the range of 30–100 K, where the current levels are almost constant, is like that of mobility, as this qualitative application of the theory says it should be. The increase in the maximum percentage of modulation at 4.2 K, Fig. 6, which is contrary to this argument, is probably a result of the total current being much higher at 4.2 K than it is at the higher temperatures, Figs. 3 and 4. Why the total current is so high at 4 K is not understood.

The theory can also explain the difference shown by Fig. 15 in the spontaneous and the driven $m=0$ oscillations. The decrease in the frequency of the spontaneous oscillations with time is caused by the increase in the temperature of the outer region of the pinch with time according to theory, Fig. 6 in I.

The driven frequency is adjusted to fall within the range that can be amplified at a given set of power input and ambient temperature conditions. This range is larger for longer-duration pulses, since the outer temperature has more time to increase and thus be appropriate for oscillations at still lower frequencies, Fig. 6 in I. The driven frequency which has time to be most amplified is the frequency which is most favorable for amplification at the outer temperature developed at the end of the pulse. The growth of driven oscillations is never extremely large, just as the growth of spontaneous oscillations is not, both for the same reason: The conditions controlling amplification are changing with time because the outer region of the pinch changes temperature with time. In Fig. 15 the current level for the driven and spontaneous oscillations is approximately equal. The driven frequency, 5.9 MHz, is the same as the spontaneous frequency at the end of the pulse. The amplitude of the driven oscillation at this frequency

(5.9 MHz) grows slowly with time, in qualitative agreement with theory.

The variation of the amplitude with total current, Fig. 5, is also consistent with theory. The well-defined current-threshold condition is the result of a marked increase in plasma density as thermal ionization on the axis dominates conduction. Further increase in the current level causes oscillations whose amplitude is governed by the inner-region current and outer-region temperature as given by the $\Gamma=0+$ condition, Eq. (25) in I. The oscillations disappear gradually as the current is increased, Fig. 5, because the growth rate becomes negative as the following reasoning shows: According to Eq. (10) in I, the inner current I_i is proportional to the mobility in this region. At the high-field conditions in the cutoff range, the mobility decreases more steeply with temperature than $T_i^{-3/2}$ (hot-electron effect). Thus, in the cutoff range, I_i is smaller than the value given by (10) in I. This causes the growth rate to become negative since $\Gamma \propto c_1 I_i^2 - c_2 T_i^{3/2}$, where c_1 and c_2 are given by Eq. (26) in I.

B. Results Not Predicted by Theory

Although the theory can satisfactorily explain most of the characteristics of the pinch oscillation for the $m=0$ mode, there are still many results which cannot be predicted by this simple theory.

The most striking property of the pinch oscillations which is not treated by the theory is the spatial growth of the percentage of modulation, $\Delta E/E$, as shown in Fig. 7. One omission of the theory which may affect spatial growth is the spatial dependence of the plasma density in the direction of current flow. The distribution of an injected plasma in the steady state has recently been measured. Thus a theory could be constructed invoking a perturbation in longitudinal direction and accounting for the plasma spatial dependence.

A second feature of the pinch oscillations not accounted for by the theory is oscillation modes other than the $m=0$ mode. Since the $m>0$ modes are present in both spontaneous and driven oscillations (even though only $m=0$ mode waves are launched), it is possible that the pinch column is deformed into sausage and helical modes before the oscillations are detectable. A more general theory is needed in which a perturbation of the form $\exp[i(\omega t+m\theta+kz)]$ should be used. This, however, introduces many difficulties in the formulation of the theory.

Third, the effect of an applied magnetic field on the pinch oscillations is quite remarkable and is neglected by the magnetothermal pinch theory. As shown in Sec. III A 5 the amplitude of the oscillations at low current levels decreases with magnetic field, reaching a minimum value at the critical magnetic field. According to Ando and Glicksman[15] the helical instability has a growth rate greater than the "pinching growth rate" when a sufficient longitudinal magnetic field is applied. Since pinching is inhibited by the helical instability, the plasma tends to remain in the unpinched state in the presence of such a magnetic field, and the oscillation caused by the magnetothermal pinch is stabilized. In fact, at magnetic fields greater than the critical magnetic field, a helical instability is excited in agreement with Ando and Glicksman's observations.[15] However, why the amplitude of the pinch oscillation is markedly enhanced at high current levels in applied magnetic fields just below the critical value, Fig. 13, is still unknown.

C. Applications

The pinch oscillation phenomena may have several applications.

A stable spontaneous pinch oscillation without an applied magnetic field is mainly a $m=0$ mode whose frequency can be varied by changing the total current. With the applied magnetic field in the range 100–500 G, the $m=0$ pinch oscillation changes to a nearly pure, stable $m=1$ mode oscillation. Therefore, a very compact signal generator which can deliver either a nearly pure $m=0$ mode or a nearly pure $m=1$ mode can be made. If the current is biased just below the threshold of the spontaneous pinch oscillation, a launched $m=0$ mode can be made to grow, whereas a launched $m=1$ mode is heavily attenuated. This phenomenon may be useful as an amplifying phase detector.

In summary, extensive data on the pinch oscillation in injected electron-hole plasmas in InSb agree well with the magnetothermal pinch theory. Several properties of the oscillations can be explained only by a more elaborate theory.

ACKNOWLEDGMENTS

The authors wish to express their gratitude to Hans-Jacob Fossum for his design of the delicate movable four-probe system, and to Robert Boice and Robert Lantz for their expert technical assistance.

---

* Work done in partial fulfillment of the requirements for the PhD degree at the University of Washington.

† Research in the Department of Electrical Engineering is partially supported by the National Science Foundation.

[1] B. Ancker-Johnson, R. W. Cohen, and M. Glicksman, Phys. Rev. **124**, 1795 (1961).

[2] M. Glicksman and M. C. Steele, Phys. Rev. **110**, 1204 (1958); B. Ancker-Johnson, J. Phys. Soc. Japan **22**, 1156 (1967).

[3] B. Ancker-Johnson, in *Seimconductors and Semimetals, 1*, edited by R. K. Willardson and A. C. Beer (Academic, New York, 1966). A review of the pinch effect is presented on pp. 433–453.

[4] A. G. Chynoweth and A. A. Murray, Phys. Rev. **123,** 515 (1961).
[5] M. Glicksman and R. A. Powlus, Phys. Rev. **121,** 1659 (1961).
[6] B. D. Osipov and A. N. Khvoshchev, Zh. Eksperim. i Teor. Fiz. **43,** 1179 (1962) [Soviet Phys. JETP **16,** 833 (1963)].
[7] B. Ancker-Johnson, in *Proceedings of the International Conference on Physics of Semiconductors, Exeter* (The Institute of Physics and the Physical Society, London, 1962), p. 131.
[8] M. Toda, Japan. J. Appl. Phys. **2,** 467 (1963).
[9] B. Ancker-Johnson, Phys. Rev. Letters **9,** 485 (1962).
[10] B. B. Kadomtsev, in *Reviews of Plasma Physics, 2,* edited by Acad. M. A. Leontovich (Consultants Bureau, New York, 1966), p. 153.
[11] C. Hilsun and A. C. Rose-Innes, *Semiconducting III-V Compounds* (Pergamon, New York, 1961), p. 126.
[12] L. V. Dubovoi and V. G. Shanskii, Zh. Eksperim. i Teor. Fiz. **56,** 766 (1969) [Soviet Phys. JETP **29,** 416 (1969)].
[13] W. S. Chen and B. Ancker-Johnson, in Proceedings of the Conference on Pulsed, High-Density Plasmas, Los Alamos, 1967 (unpublished); Bull. Am. Phys. Soc. **12,** 712 (1967); A. P. Shotov, S. P. Grishechkina, and R. A. Muminov, Zh. Eksperim. i Teor. Fiz. **52,** 71, (1967) [Soviet Phys. JETP **25,** 45 (1967)].
[14] W. S. Chen and B. Ancker-Johnson, Appl. Phys. Letters **15,** 59 (1969).
[15] K. Ando and M. Glicksman, Phys. Rev. **154,** 316 (1967).

PHYSICAL REVIEW B VOLUME 2, NUMBER 11 1 DECEMBER 1970

Ettingshausen Effect in the Intermediate State of Thin Superconducting Pb Films*

V. A. Rowe and R. P. Huebener
Argonne National Laboratory, Argonne, Illinois 60439

(Received 1 June 1970)

Earlier measurements of the Nernst effect in thin films of Pb, Sn, and In have shown that below a critical film thickness d_c, the entropy per unit length and per unit flux transported by the vortices decreases strongly with decreasing film thickness. To check this behavior, we have measured the Ettingshausen effect in the intermediate state of superconducting Pb films at 4.2 K as a function of the magnetic field. The films investigated were 0.75 and 3.16 μm thick. The Ettingshausen data clearly confirm the earlier results obtained from the Nernst effect. It is suggested that the decrease of the transport entropy with decreasing film thickness, found below d_c, is due to the increasing vortex interaction present in very thin type-I films.

I. INTRODUCTION

There is now an impressive body of evidence, theoretical[1–3] and experimental,[4–6] indicating the presence of a vortex state in thin superconducting type-I films that is distinctly different from the usual intermediate state found in thick films and foils and in bulk material. Magnetization experiments[5] demonstrate that in the case of Pb films at 4.2 K, the new state is established in films thinner than a critical thickness d_c of about 1.5 μm.

Previous thermomagnetic experiments[7] on thin films of Pb and on Sn and In using the Nernst effect showed that S_φ/φ, the entropy per unit length and per unit flux transported by the vortices, as a function of film thickness passes through a maximum between 3 and 7 μm, depending on the material, and diminishes in the thinnest films investigated. This behavior of the transport entropy for small film thickness had been explained tentatively by the increasing vortex interaction present in thin type-I films. However, the Nernst-effect measurements may be complicated by the fact that relatively large temperature gradients have to be employed leading to an appreciable nonuniformity of the characteristic superconducting parameters across the sample. This complication can be avoided in an experiment which measures the Ettingshausen effect.[8] In order to confirm our earlier results from the Nernst effect on the transport entropy in thin type-I films, we have studied the Ettingshausen effect in Pb films of 0.75 and 3.16 μm thickness. The Ettingshausen measurements clearly confirmed that, below a critical film thickness, the transport entropy in type-I films diminishes with decreasing film thickness.

II. EXPERIMENTAL TECHNIQUES

Figure 1 shows schematically how the samples and the electronics were arranged for the Ettingshausen experiments. The samples were made by evaporation of 99.999% pure Pb [9] from a Joule-heated tantalum boat in a vacuum of 10^{-5} Torr or lower. Microscope slides 1 mm thick were cut to 3.8×1.3 cm and masked by a thin-foil shadow mask produced by photo reduction and etching techniques. Niobium potential and copper current leads were soldered with pure In to the substrate prior to the deposition. Film thickness was measured by weighing thin cover glass slides on a microbalance before and after the film deposition. The distance between heat sinks was 2.54 cm, the distance between voltage probes was 2.28 cm, and the film width was 0.96 cm. The substrates were cleaned in a three-step process: They were first scrubbed with detergent, then placed in an ultrasonic cleaner with ethyl alcohol, and